

Electric Potential and Electric Field Imaging with Applications

by E.R. Generazio*

ABSTRACT

The technology and techniques for remote quantitative imaging of electrostatic potentials and electrostatic fields in and around objects and in free space is presented. Electric field imaging (EFI) technology may be applied to characterize intrinsic or existing electric potentials and electric fields, or an externally generated electrostatic field may be used for “illuminating” volumes to be inspected with EFI. The baseline sensor technology, electric field sensor (e-sensor), and its construction, optional electric field generation (quasi-static generator), and current e-sensor enhancements (ephemeral e-sensor) are discussed. Demonstrations for structural, electronic, human, and memory applications are shown. This new EFI capability is demonstrated to reveal characterization of electric charge distribution, creating a new field of study that embraces areas of interest including electrostatic discharge mitigation, crime scene forensics, design and materials selection for advanced sensors, dielectric morphology of structures, inspection of containers, inspection for hidden objects, tether integrity, organic molecular memory, and medical diagnostic and treatment efficacy applications such as cardiac polarization wave propagation and electromyography imaging.

KEYWORDS: nondestructive evaluation, nondestructive testing, electric potential, electric field, charge distribution, triboelectric, electrostatic discharge.

Introduction

Direct imaging of electrostatic potentials and electrostatic fields eluded researchers for many years. Prior general applications used a series of potential measurements over a path of resistance supporting a current (Sothcott, 1984; Yang and Macnae, 2002). One popular example uses conductive electrodes drawn on a resistive sheet that are held at some potential difference. The voltage potential between points is mapped from which electric field lines may be drawn in a plane. Even for this simple case, the actual current path over the resistive sheet is unknown, and the electric field exists in three dimensions so the true electrostatic field is not quantified. These techniques estimate the apparent resistivity rather than specifying the electrostatic field.

A basic problem when attempting to image electrostatic fields is that the measurement sensor is composed of materials that distort the electric field to be measured. Dielectric, conductive, semi-conductive, insulating, and triboelectric materials all distort the original true electric field to be measured. An earlier work discusses the complexities of measuring scalar potentials and electric fields and provides an optical technique based on optical phase shift for determining electric field distributions (Zahn, 1994). Researchers have demonstrated quantitative techniques to measure electronic signatures of electrostatic fields (Blum, 2012; Dower, 1995; Hassanzadeh et al., 1990). However, measurement of the electronic signature is not a quantitative metric of the true electric field, so correlations are made to identify objects of interest and so on. Inaccuracies in prior measurements arose due to the lack in attention to detail describing the construction of the sensor, the electronic components, and the supporting structures.

This work describes techniques to measure the electrostatic potential and electrostatic field emanating from an object or existing in free space using the electric field sensor (e-sensor) design described elsewhere (Generazio, 2011). Subsequent work describes the construction of a quasi-static electric field generator that “illuminates” large volumes with a uniform electrostatic field, including in U.S. patent application No. 13/800379, titled “Quasi-static Electric Field Generator,” filed by the author in 2013 (Melcher, 1981; NASA, 2014).

* Ph.D., National Aeronautics and Space Administration, Hampton, Virginia 23681.

Specifically, these two inventions allow for the quantitative determination of the true metric of the electrostatic field emanating from or passing through or around objects and volumes. The inventions provide quantitative metrics of the electrostatic potential, electrostatic field strength, spatial direction of the electrostatic field, and spatial components of the electrostatic field.

E-sensor Circuit Challenges

A field effect transistor (FET)-based e-sensor is described that uses a non-specified FET configuration, that is, an FET-based e-sensor circuit that uses a floating gate configuration, which is contrary to all good circuit designs (Generazio, 2011). Good circuit designs that use FETs require a properly supported, but small, electrical current to exist in the gate for the FET to function per manufacturer specifications. There are three basic electronic FET configurations: common source, common drain, and common gate. FETs may be calibrated for common source and common drain configurations where the gate is physically connected to a voltage source. In the common gate configuration, the gate is physically connected to ground. In all configurations, the electrical connections to the gate are at an electrical potential that is a direct physical electrical path for charged carriers. The e-sensor described here does not provide the required physical connection for the specified gate current.

When an FET is used in a floating gate configuration, gain stability difficulties arise that inhibit calibration. Floating gate-based designs require unique calibration protocols. Two aspects to this calibration are the voltage gain and time response of the e-sensor circuit in the presence of a non-direct static and quasi-static electric potential. The manufacturing tolerance of FET characteristics is well known, making uniform calibration of multiple FET floating gate-based sensors for array-based configurations even more challenging (Horowitz and Hill, 1989).

E-sensor Construction

Figure 1 shows the basic e-sensor circuit elements. Other floating gate-based circuits may be used. In addition to the electronic elements of the circuit, attention must be given to all materials used in the construction of the sensor for the production of a useful measurement system. It is preferable to avoid the occurrence of all surface charges (bound and free) and image charges near the sensing gate of the FET, electronic connections, and supporting structures. The e-sensor components need to be triboelectrically neutral, have low electric susceptibility, and be non-conducting to minimize sensor distortions of the true electric field due to charging, dielectric polarization, and free carrier polarization. Further details of e-sensor design are available elsewhere (Generazio, 2011).

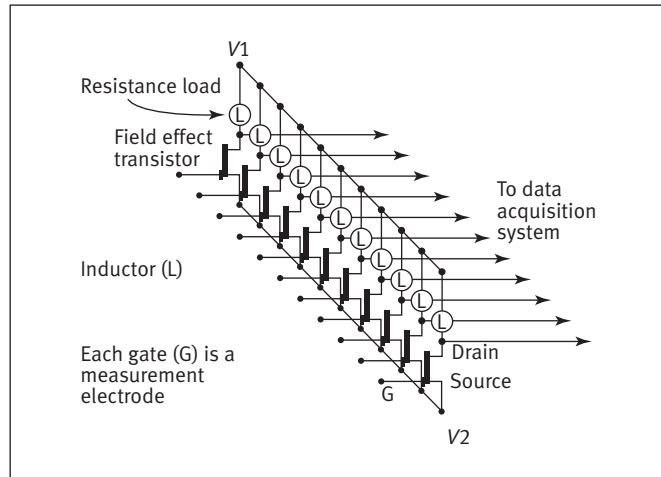


Figure 1. Schematic diagram of an array of electric field sensor circuit elements.

Figure 2 shows the measurement response of a 16-element e-sensor array. Note that the measurement voltage is not the electrostatic potential. The electrostatic potential is obtained via calibration, and calibration parameters vary for each e-sensor. In practice, all e-sensors are calibrated before every scan by generating a slowly oscillating uniform potential across the e-sensor array. Typical electrical potentials measured are a few volts with a noise level of ± 5 mV, yielding high signal-to-noise ratios that exceed 700. Here, the electrostatic potential at the e-sensor gates is slowly varied at a 2 Hz rate by a remote rotating electrostatic dipole. If the potential is held fixed at any point in time, the measured potential at the e-sensor slowly drifts to an e-sensor equilibrium voltage. Each e-sensor has a different equilibrium voltage and a

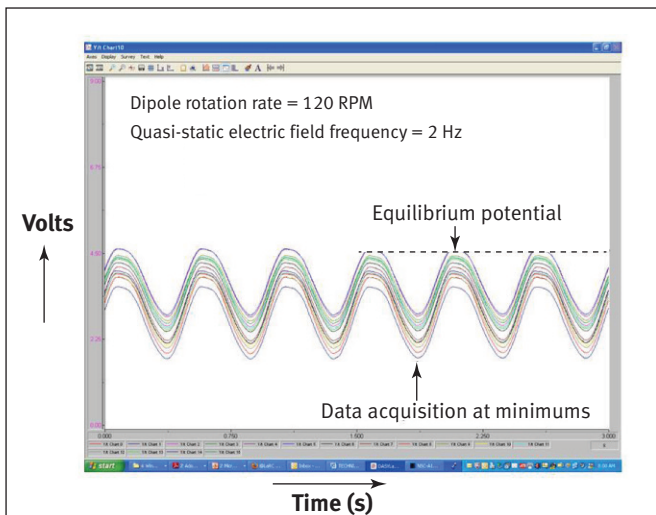


Figure 2. Example measured output from 16 electric field sensors in the presence of a reference quasi-static electric field.

different characteristic time to reach an equilibrium voltage. Typical times to reach equilibrium are a few to several seconds and are dependant on how well the e-sensor design meets the requirements identified earlier. The best designs will exhibit minimal drift. It is important to note here that the equilibrium potential value is independent of any external potential on the floating gate. The equilibrium potential for the topmost signal in Figure 2 is shown. The effect of leakage currents may be recognized by the non-sinusoidal potential response at the peaks of the e-sensor outputs. Each peak shape is different, where some are rounded and others are flattened or sloped. These slight variations are due to leakage currents making calibration efforts challenging. The origin of this effect is broadly described to be charging of the gate of the FET due to leakage currents. A more detailed discussion on leakage effects requires an evaluation of parasitic capacitances, inductances, and resistances of the entire e-sensor and structural support system. It is defined here that the phrase “effects due to leakage currents” refers to all effects related to intrinsic electronic properties, including leakage of free carriers across electronically insulated boundaries, free carrier buildup, free carrier charging, and all parasitic capacitances, inductances, and impedances. Intrinsic refers to dimensionally changing volumes of coverage. The volume of coverage starts at the solid state level, goes through the solid state mounting to reach the support structure levels, and advances to describe an electrostatic potential and field sensor for general applications. For example, the structural supports of the solid-state elements have dielectric properties and therefore have intrinsic parasitic capacitance, similarly for the structural support of the structure supporting the solid-state element, and so on.

The quasi-static electric field generator is designed to provide a controlled source or reference quasi-static electric field for “illumination of objects and volumes” and to reverse and minimize the effects of sensor and support structure parasitic leakage currents. At a quasi-static frequency of 3 Hz, the minimization is adequate so that gain is controlled and the calibration of gain of the e-sensor in a quasi-static electric field is straightforward.

The quasi-static frequency range is defined where the electric field is present at the gate electrode of the FET for a long enough time for the e-sensor response to reach a steady state for potential measurement, but not long enough for intrinsic and extrinsic leakage or oscillating currents to dominate the measurement of the true static potential. In the defined quasi-static frequency range, accurate metric measurements of the true static potentials are made from which the true static electric field is obtained.

The generator consists of a rotating electrostatic dipole (Figure 3) to generate a slowly varying electrostatic potential. The dipole is charged using a triboelectric process similar to a van de graaff generator. The dipole charging system is battery powered and wirelessly controlled. All power, wireless

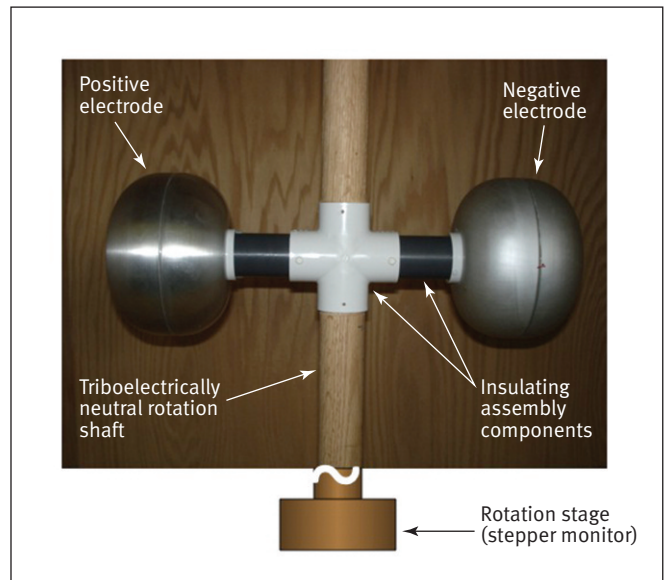


Figure 3. Photograph of the rotating quasi-static dipole element.

receiver, and speed controllers are contained within the structure of the dipole element. A dry wood construction approach is used to maintain the uniformity of the electric field in the vicinity of the dipole. Wood having neutral triboelectric affinity and low dielectric properties is used to limit stray charging and polarization of the structure of the generator and for the rotational support of the dipole. A large conducting plate (see Figure 4) is used to establish an equipotential surface and uniform electrostatic field when used in a near field approximation configuration. The dipole is rotated by a computer controlled stepper motor at quasi-static frequencies to provide a slowly varying uniform electrostatic field. Other approaches may also be used to generate an electrostatic field. However, the approach described here is human safe operating at 100 000 V while providing only microamperes of current and is isolated from building power supply systems.

Electric Field Imaging System

The electric field imaging (EFI) system configuration for inspections is shown in Figure 4. In this configuration, the object being inspected is moved, via a conveyor, to pass between the quasi-static generator and a linear array of e-sensors. During movement of the object, the dipole may be rotating at any desired speed. Speeds below the quasi-static range may be used to explore leakage effects of material and structural configurations. Speeds just above the quasi-static range are extremely low frequency (ELF) electromagnetic waves (ITU, 2000). ELF and higher frequencies exhibit radiative electromagnetic propagation effects that need to be included in the analysis. Data acquisition of the e-sensor response may be performed when a preselected voltage, V_{surface} , occurs on the conducting surface, or throughout the

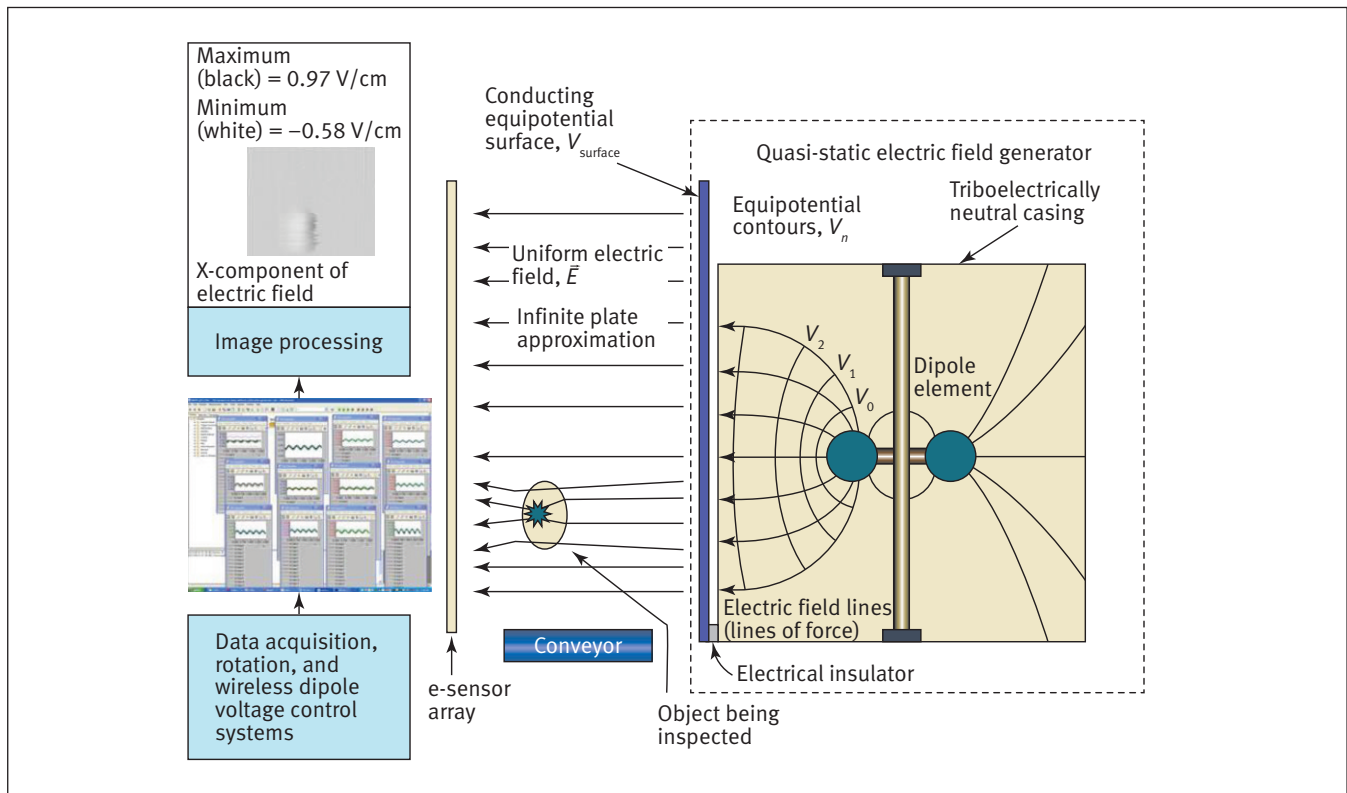


Figure 4. Diagram of the setup for the electric field imaging (EFI) system. The EFI system consists of a linear array of electric field sensors (e-sensors), a quasi-static electric field generator, a conveyor, a data acquisition and image processing system, and an object to be inspected.

cycle of the dipole rotation. Data acquired at a preselected voltage correspond to a constant interrogation electric field strength. Data acquired during the rotational period of the dipole correspond to a varying interrogating electric field magnitude. For the image data shown here, the potential data are acquired at the times when the dipole is at the same orientation so that V_{surface} is at a constant value during measurements. The orientation at data acquisition corresponds to the voltage minimums shown in Figure 2.

A 914 mm long vertical linear array of 192 e-sensors is placed 457 mm from the conducting plate of the quasi-static generator providing a uniform electric field. Plates having dimensions of 60.96×121.92 cm and 121.92×243.84 cm are adequate to generate uniform electric fields of the inspection region. During inspection, the object, at a fixed position along the Z axis, is moved by the conveyor along the X axis. The acquired data from the e-sensor array oriented along the Y axis may be processed to generate images of the electric field from the object being inspected (Generazio, 2011). The e-sensor array may be moved along the Z axis by computer control. Data obtained with the e-sensor array at two or more positions along the Z axis provide sufficient information to generate images of the electric field. Each scan measures the electrostatic potential in the X-Y plane to generate an electrostatic potential image. EFI reconstructions are produced using

the electrostatic potential images. Many other scanning and e-sensor array configurations are possible.

Examples of Electric Field Imaging Images

The capability to image the electrical potential and electrical fields emanating from objects opens a wide range of possible applications. In some EFI evaluations, only the electric potential is needed, while other applications will benefit from determining the electric field. The following describes the first EFI application on a human and the detailed analyses technique for determining the electric field. Representative EFI applications are presented for evaluating complex structural components, construction materials, and for supporting crime scene forensics, electrostatic discharge (ESD) mitigation, and for the development of a molecular memory.

Human in a Uniform Electrostatic Field

Figure 5a shows the electrostatic potential of a human in a uniform electrostatic field. The image linear gray scale represents the electrostatic potential ranges from 0 V (dark shade) to -3.75 V (light shade). This is one of the first images obtained with the EFI system. It was originally thought that the dipole would need to be constantly triboelectrically charged to maintain a constant potential on the electrodes of the dipole. The effect of that constant charging is shown as

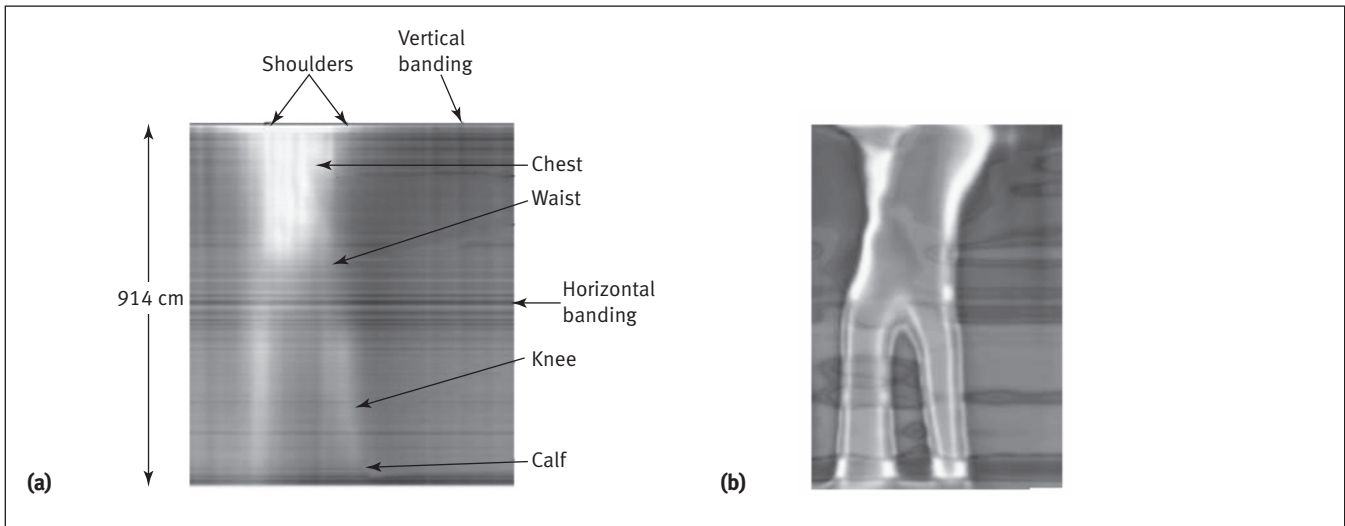


Figure 5. Image of a human: (a) electrical potential image in a uniform electric field; and (b) commercially available graphics filter applied to the potential data shown in Figure 5a.

vertical banding in this image. It is now known that, for this structural design, the dipole will hold a constant charge for several hours so constant charging is not needed, and these vertical bands do not appear in subsequent images. The horizontal lines are due to variations in the individual e-sensor responses that are not fully removed by calibration procedures. The sensor-to-sensor variations are due to residual gate charging and work to address this charging has led to the development of a more accurate ephemeral e-sensor that is presented later.

Figure 5a is presented here as the first image obtained showing the electrostatic potential of a human in a uniform electrostatic field. A detailed physics-based imaging processing procedure was developed and subsequently used for the data to follow. A commercially available graphic filter is applied to the potential data (Figure 5a) and reveals (Figure 5b) a striking amount of information suggesting the presence of a straight cut cotton shirt, cotton pants, legs, and stretchy (containing polymer materials) socks. The graphic filter routine highlights image intensity and intensity gradients and is not meant to be representative of an electric field image.

Hybrid Composite in a Uniform Electrostatic Field

The electric potential of a hybrid composite compression test specimen is shown in Figure 6. The test specimen has top and bottom support brackets and has a 3.0 cm thick crushed metallic honeycomb core and cracked and buckled composite faceplates. The EFI system reveals that the test sample is redirecting the uniform electric field to change the original uniform electrostatic potential (light gray shade in the upper edge of Figure 6c) so that electric potential is raised (dark shade) in the free space around the test specimen. In literal contrast, the electric potential is raised (darker shade) over the test object with some decreased (lighter shade) potential

variations existing horizontally across the central region of the test specimen. The top and bottom support brackets have the largest decrement in electrostatic potential (light shade). The image has a linear gray scale representing the electrostatic potential ranges from 0.0 V (dark shade) to -3.73 V (light shade). Polarization of the specimen is also revealed as decrements (light shades in Figure 6c) and increments (dark shades in Figure 6c). The 3D graphical representations (Figure 6d and 6e) of the gray scale plot of electrostatic potential (Figure 6c) highlights how the object distorts the equipotential in which it is placed. The large horizontal bands represent the electrostatic potential of the upper and lower specimen brackets. Figure 6e shows the 3D representation of the electric potential as viewed at a 45° angle.

Electrostatic Field Imaging

The generation of electric field images from the electrostatic potential data is described. The electrostatic potentials of the hybrid composite test specimen at two different Z axis locations spaced 1 cm apart (labeled near and away from the e-sensor array) are shown on the left hand side of Figure 7. The electric field, \vec{E} , and electric field spatial components, \vec{E}_x , \vec{E}_y , and \vec{E}_z , are obtained using the relation:

$$(1) \quad \vec{E}(X,Y,Z) = -\nabla V(X,Y,Z) = -\left(\frac{\partial V[X,Y,Z]}{\partial x} \hat{i} + \frac{\partial V[X,Y,Z]}{\partial y} \hat{j} + \frac{\partial V[X,Y,Z]}{\partial z} \hat{k} \right)$$

where

$V(X,Y,Z)$ is the measured electrostatic potential with X, Y, and Z coordinates, \hat{i} , \hat{j} , and \hat{k} are unit vectors in the X, Y, and Z directions, respectively.

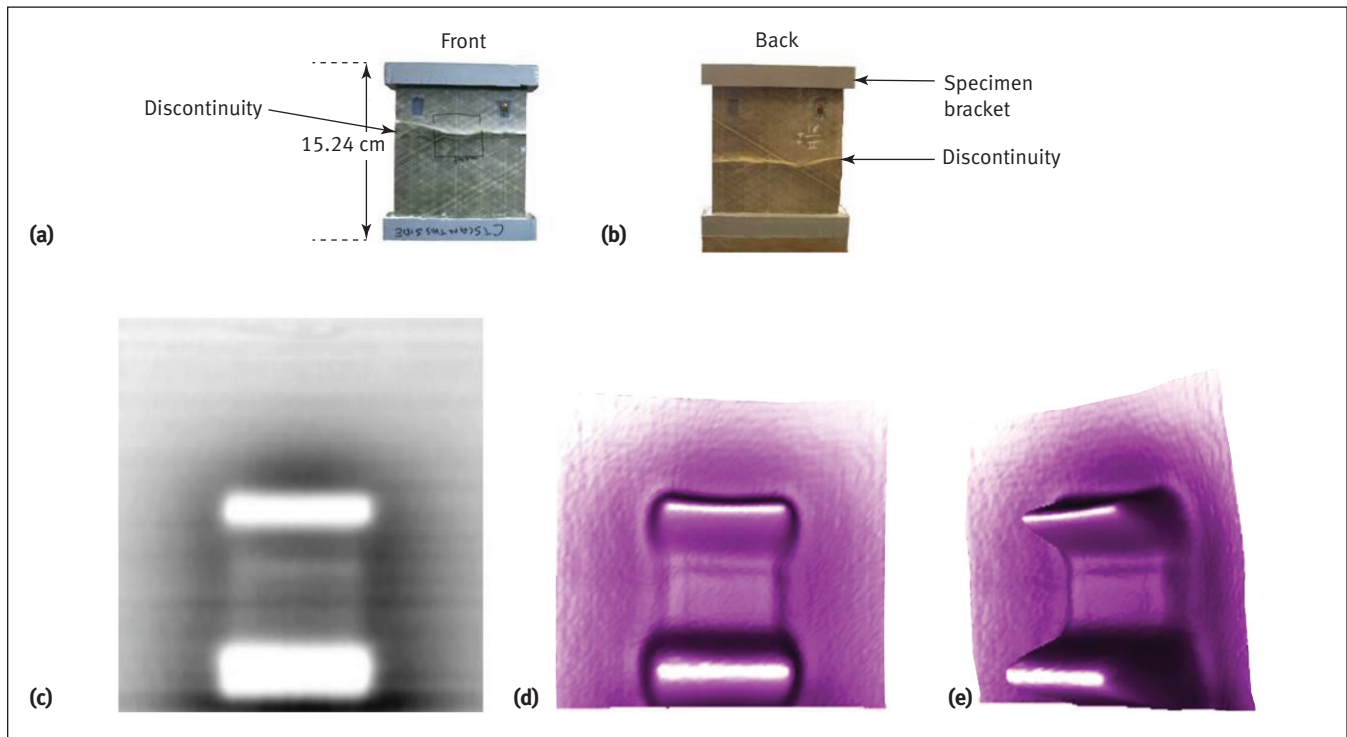


Figure 6. Hybrid composite compression test specimen: (a) front image; (b) back image; (c) electrostatic potential of a hybrid composite in a uniform electric field; (d) electrostatic potential 3D graphical representation; and (e) electrostatic potential 3D graphical representation rotated 45°.

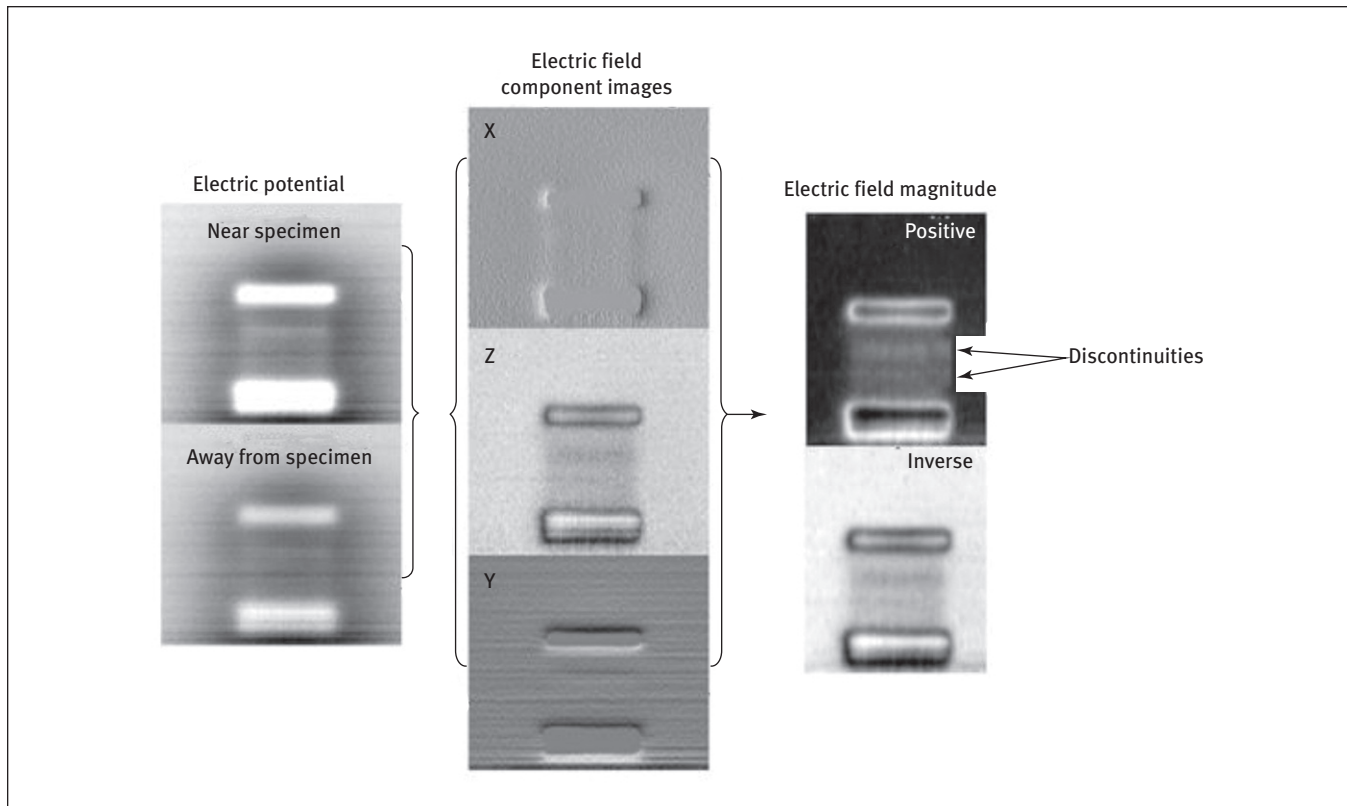


Figure 7. The electrostatic potential of a hybrid composite specimen in a uniform electric field. The electrostatic potentials are measured at two different distances from the specimen. Images of the X, Y, and Z components of the electric field and of the electric field magnitude are shown.

Equation 1 is approximated for any point $X_i, Y_i,$ or Z_i .

$$(2) \quad \vec{E}(X_i, Y_i, Z_i) \approx - \left[\begin{array}{l} \left[\frac{V(X_{i+1}, Y_i, Z_i) - V(X_i, Y_i, Z_i)}{X_{i+1} - X_i} \right] \hat{i} + \\ \left[\frac{V(X_i, Y_{i+1}, Z_i) - V(X_i, Y_i, Z_i)}{Y_{i+1} - Y_i} \right] \hat{j} + \\ \left[\frac{V(X_i, Y_i, Z_{i+1}) - V(X_i, Y_i, Z_i)}{Z_{i+1} - Z_i} \right] \hat{k} \end{array} \right]$$

It is instructive to show images of the electric field components as an interim analysis step in Figure 7. Figure 7 shows plots on a gray scale of the components of the electric field along the X, Y, and Z directions. The Y-component of the electric field exhibits discrete horizontal banding that crosses the entire image and is due to the incomplete sensor-to-sensor calibration made more apparent by the approximation of the equation. The electric field is given by the vector sum of the components, $\vec{E} = \vec{E}_x + \vec{E}_y + \vec{E}_z$, and has an electric field magnitude, $|\vec{E}|$ shown in Figure 7. The electrostatic field magnitude positive image has a linear gray scale and ranges from 0 V/cm (dark shade) to 2.275 V/cm (light shade). The positive and inverse labels in Figure 7 refer to the image reproduction for display visualization. It can be seen from the electric field magnitude positive image in Figure 7 that there are high electrostatic fields (light shade) present at the perimeter of the test specimen brackets as well as between the brackets. The black areas of the electrostatic field magnitude positive image represent low electrostatic field intensity; there remains an electrostatic potential in these areas, but the electrostatic gradients are minimal. High electrostatic fields are expected to occur at potential arcing sites.

Insulated Connection Cabling and Integrated Circuit Component in a Uniform Electrostatic Field

Next, the EFI capability on other systems is explored to show the utility in other applications and for guidance in sensor designs. The effect of cabling and shielding on measurements is well known; however, little attention is paid to the effect on sensor capability. The electrostatic potential distortions of a coaxial cable and an integrated circuit are shown in Figures 8a and 8b. The range of linear gray scale shading is listed in Figure 8. Both of these standard circuit components dramatically distort electrostatic fields for large distances. The cable increases the electrostatic potential while the integrated circuit decreases the electrostatic potential. A comparison of insulation materials is shown in Figure 8c, where an ungrounded #38 magnet wire does not distort the applied electrostatic potential, V_0 , to a measurable amount. In contrast, polyvinyl chloride, cotton, rayon, and polyethylene insulation around the magnet wire all produce significant

changes in the potential. The apparent shading in this image is due to surface charge on the insulation from handling and is discussed later. When developing advanced remote sensors, for example, those used in medical applications, the impact of all the components of the sensor needs to be addressed.

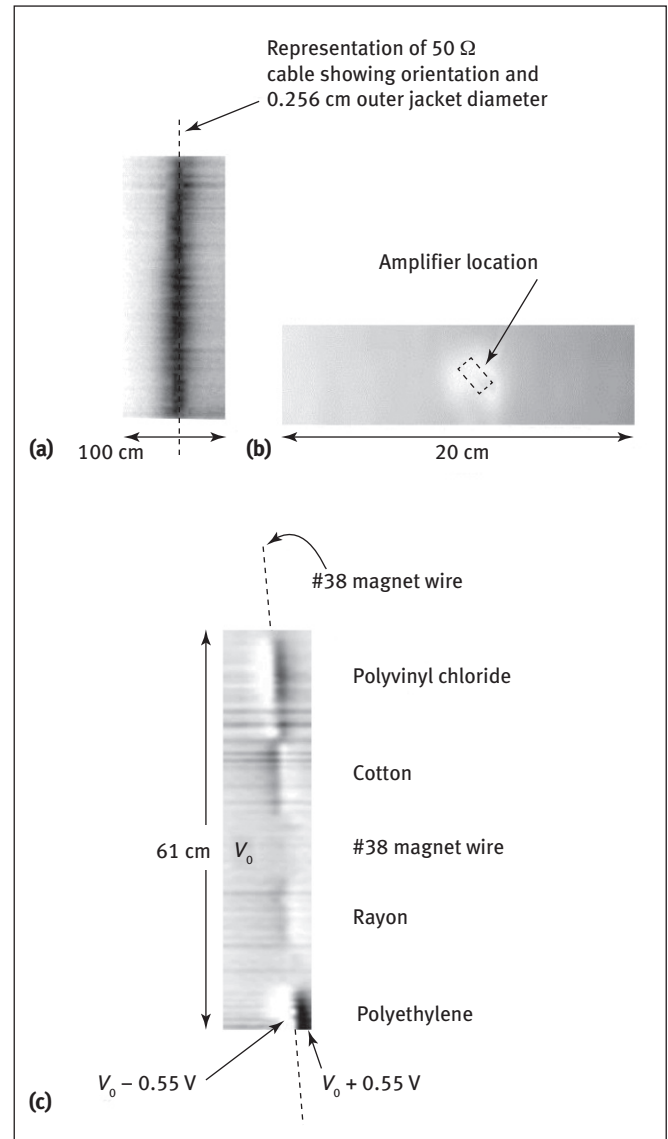


Figure 8. Electrostatic potential image: (a) coaxial cable; (b) integrated circuit in a uniform electric field; and (c) wire, having different insulation materials, in a uniform electric field. In Figure 8a the cable is carrying no current and creates electrostatic potential distortions at extremely large spatial distances, compared to the cable diameter, from the cable. The electrostatic potential around the cable ranges from -3 V (lightest areas) to -2 V (darkest areas). In Figure 8b, the dual inline package (DIP) operational amplifier is oriented so that the DIP's 10 × 20 mm top surface is normal to the reference electric field direction. The operational amplifier creates electrostatic potential distortions at extremely large spatial distances, compared to the amplifier dimensions. The electrostatic potential around the amplifier ranges from -3 V (darkest areas) to -4 V (lightest areas).

Construction Materials in a Uniform Electrostatic Field

ESD is a well-known field and there are substantial industrial investments in addressing and mitigating ESD issues in manufacturing and product use. Electrostatic potential images generated by EFI of selected materials are shown in Figure 9 and Table 1 along with the companion dielectric constants and triboelectric affinities. Figure 9a shows the electrostatic potential image for 25.4 mm diameter as received rods of different materials. Here again the strong effect that conducting materials have on the electrostatic potential is recognized by the increase in potential (large dark shaded area on the right side of the image) near the copper rod. The linear gray scale ranges from 0.0 V (dark shade) to -4.79 V (light shade). The effect is so strong that the other rods are embedded in an electrostatic potential modified by the copper rod.

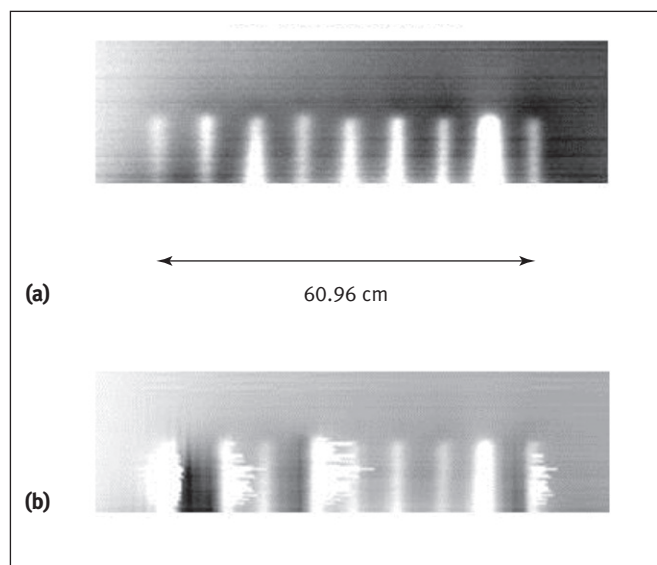


Figure 9. Electrostatic potential image of solid rods of different materials in a uniform electric field: (a) as received; and (b) after being brushed once with a silk cloth. The materials shown cover a wide range of dielectric constants and triboelectric affinities.

TABLE 1
Dielectric constants of samples shown in Figure 9*

| Dielectric constant ϵ | Material | Triboelectric affinity |
|-----------------------------------|---------------------------|------------------------|
| 2.0–2.1 | PTFE [†] | -190 |
| 2.7 | Acrylic | -10 |
| 1.2–2.1 | Wood | +7 |
| 3 | Nylon | +30 |
| 4.5–5 | Fiberglass-epoxy laminate | +30 |
| 4–9 | Mica ceramic | - |
| 3.8 | Borosilicate glass | +25 |
| - | Copper | ~0 |
| 2.8–4.1 | Polyester | -40 |

* Samples are in order from left; † PTFE = polytetrafluoroethylene.

The same rods were brushed once with a silk cloth. The electrostatic potential image in Figure 9b shows the electrostatic potential image for the rods after being brushed by the silk cloth. Here the polytetrafluoroethylene (PTFE), acrylic, nylon, and polyester rods are charged by the triboelectric interaction with the silk cloth. The triboelectric charging is of sufficient magnitude that the resulting electrostatic potential saturates the e-sensors. The charged gates of the e-sensors recover slowly during the scan and leave a record of this recovery by producing both an increased potential (dark shadow) and decreased potential (light shadow) adjacent to the affected rods. Similar shadowing is observed in Figure 8c.

Electrostatic Field Imaging for the Development of Organic Memory

The preceding results are quite interesting where it is observed that the triboelectric charges on the rods lingered for long periods of time. PTFE had the largest magnitude charge on the potential field as expected since PTFE has the largest triboelectric affinity. During the setup of the rod sample set, it was noticed that the PTFE rod had a bright spot (decreased electrostatic potential) on the top on the rod's electrostatic potential image. Given the observed long latency or memory times of charges on PTFE, it became clear that the previously bright spot on the PTFE rod was from triboelectric

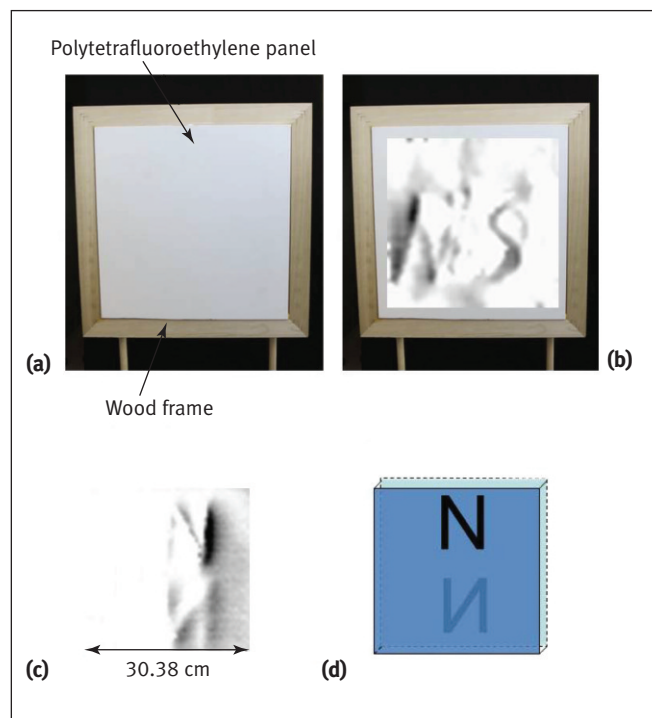


Figure 10. Evaluating the memory storage capability of organic polymers: (a) photograph of the setup; (b) triboelectrically drawn letters, "NASA," are revealed in the electrostatic potential image; (c) the electrostatic potential of the letter "N" triboelectrically hand-drawn, on two sides on a polymer sheet; and (d) schematic image of the image in Figure 10c. The sheet measured 0.64 × 30.38 × 30.38 cm.

charging, which occurred during handling and placement of the rod into the sample holder.

A memory storage device was constructed by mounting a PTFE panel in a wooden frame (Figure 10a). The letters “NASA” were drawn on the surface of the PTFE panel using a finger. The EFI potential image is shown in Figure 10b, where the letters NASA are visible. The last “A” had a large magnitude potential and almost fully saturated the e-sensors. Several techniques were used to “erase” the charges from the panel; however, in a comic moment the author found himself generating double and triple exposures over the same original writing. This image demonstrates that EFI is useful in characterizing charge distribution and EFI may also be used to monitor changes in charge distribution. This memory storage approach is an area of study that is opposite of that addressed for ESD.

EFI methodology is able to measure the electric potential from charges that are subsurface and not on the exposed surface being imaged by the e-sensor. The electrostatic potential of the letter “N” triboelectrically hand-drawn, using a finger on a polymer sheet, is shown in Figure 10c. The drawing of the letter “N” leaves residual induced charges on the surface drawn. There are two “N” letters shown in Figure 10d. One letter “N” is drawn on the upper half of the front surface and the second letter “N” is drawn on the lower half of the back

subsurface of the polymer sheet. The electrostatic potential image reveals both the “N” letters on the front and back sides of the polymer sheet. This is an important result. Even though there are no triboelectric surface charges on the front lower half of the polymer sheet, an image of the electrostatic potential of the letter “N” on the back surface is clearly observed. That is, subsurface charges may exist, and their electrostatic potential can be measured by both single- and double-sided EFI, even when the surface exposed to the e-sensor is uncharged.

The capability of EFI to characterize subsurface electric potential variations has important implications. Figure 11 shows an optical image of an acrylonitrile butadiene styrene (ABS) gun simulator in a container. The ABS gun simulator has no conducting metallic content or conducting components. The ABS gun simulator is packed, using typical foam packing materials, in a non-conducting container. The EFI electrostatic potential image is shown as a gray scale plot overlaid onto the optical image of the container. The gun simulator is identified in the electrostatic potential image (Figure 11c). The body and the barrel of the gun are clearly discernable. The simple act of packing the gun simulator changes the electrostatic potential of the gun for an extended period of time. The EFI shown in Figure 11c was obtained 24 h after packing.

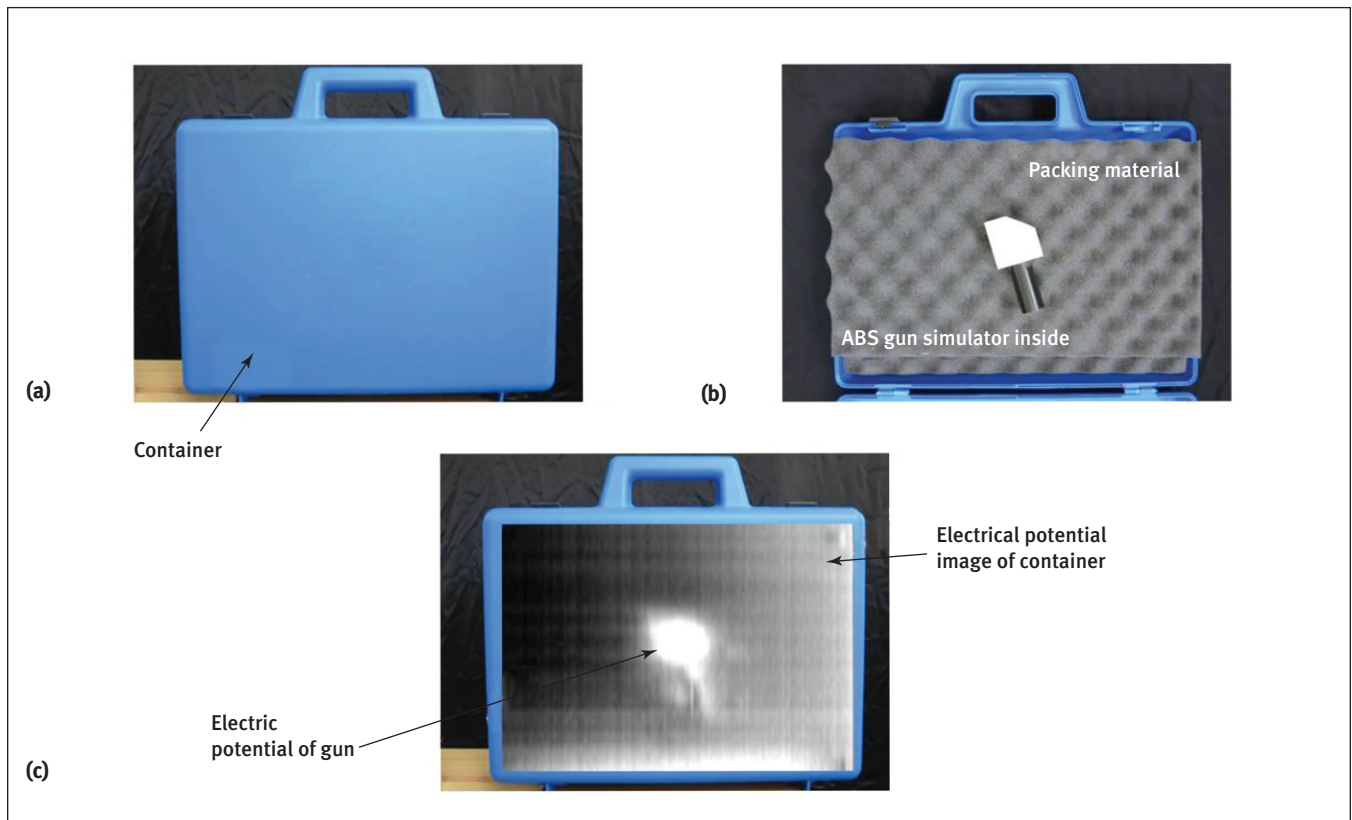


Figure 11. Acrylonitrile butadiene styrene (ABS) gun simulator in a container: (a) exterior photograph of the setup; (b) interior photograph showing the ABS gun; and (c) electrostatic potential image.

Subsequent modifications to the e-sensor design have removed the shadowing due to saturated charging and leakage effects. The modified e-sensor functions in an ephemeral

mode (Generazio, 2015). The difference between the e-sensor and the ephemeral e-sensor is that the ephemeral e-sensor is intrinsically forced to return to an uncharged state between measurements. The construction of an ephemeral e-sensor has been described in detail (Generazio, 2015). Preliminary data from an ephemeral e-sensor are presented here. Figure 12 shows the electrostatic potential, measured simultaneously by both an e-sensor and an ephemeral e-sensor, of a cylindrically symmetric object that has been charged to saturate the e-sensor. Effects due to leakage currents are absent in the potential measurements from the ephemeral e-sensor.

A solid-state ephemeral e-sensor was developed for enhanced single sided measurements and will be reported in later research. Forensic evaluations of surfaces may be performed using ephemeral e-sensors. The electric potential of an office rug changes with footfalls. Figure 13 shows electrostatic potential plots on a gray scale due to residual charges left by footsteps on an anti-static rug. The rug potential varies by -4.46 V (lightest shade in Figure 13b) after being walked on. The individual left and right footsteps are clearly identified, indicating the travel direction, as well as the manufactured tread patterns on the bottom of the shoes. Footfall imaging was done up to 30 min after travel. However, it is expected that undisturbed paths may be imaged days later depending on the materials in contact. Footfalls are only one example of forensic interest, and other forensic applications are possible. Future work in this area is needed to establish the residual charge distribution as a function of time.

Conclusion

It is important to summarize the preceding results to form a complete picture of what was learned. The construction of an e-sensor system that provides a true metric of the electric potential needed for the generation of electrostatic potential

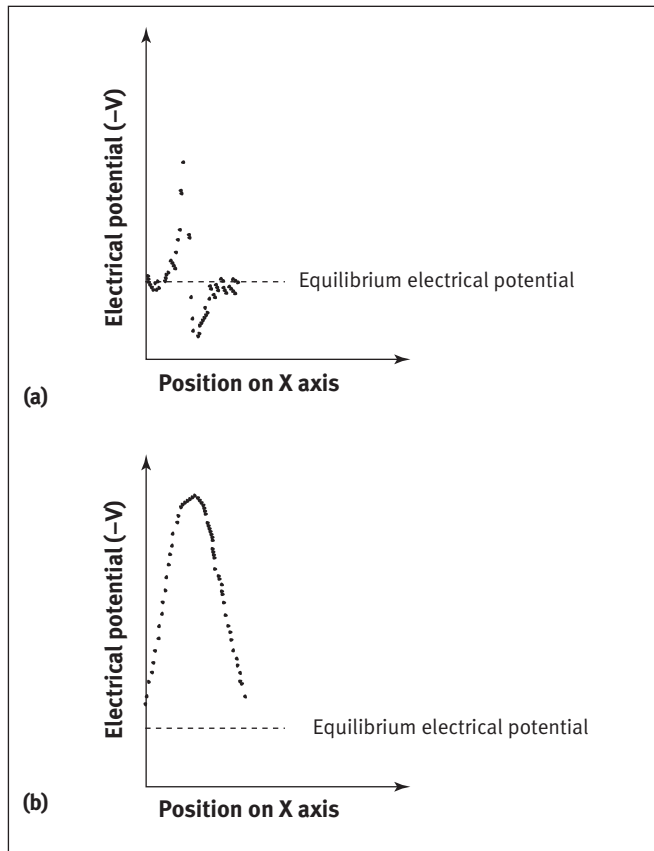


Figure 12. Electrostatic potential of a cylindrically symmetric object charged to saturate the electric field sensor (e-sensor) by: (a) an e-sensor; and (b) an ephemeral e-sensor.

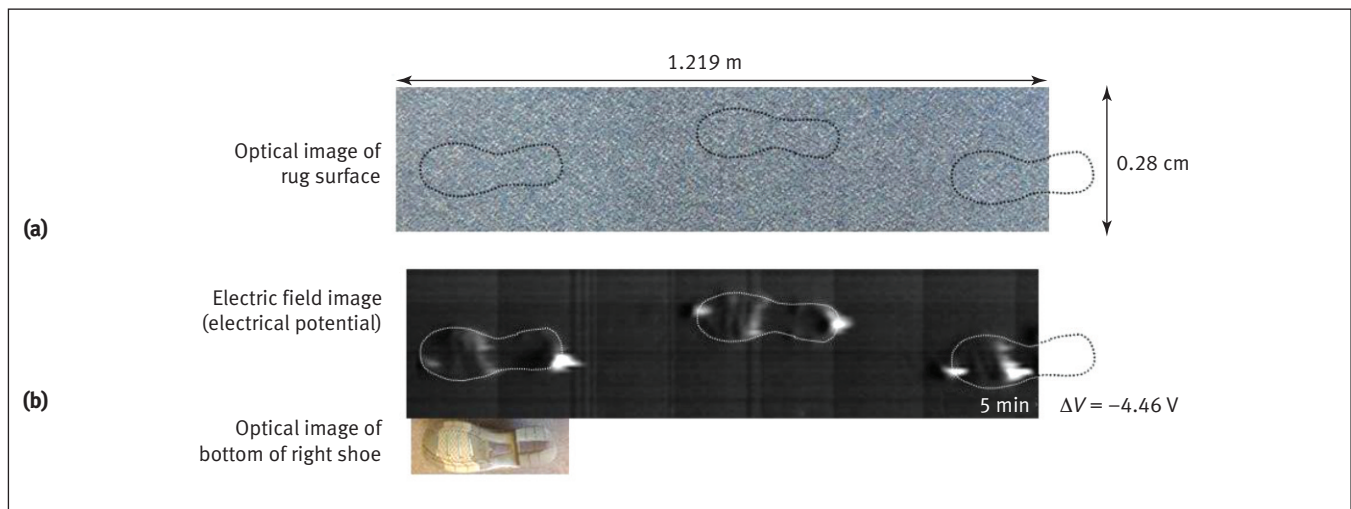


Figure 13. Forensic electrostatic potential image of footfalls on a static protection office rug: (a) photograph of rug surface; and (b) electric field image.

and EFI was presented. The construction materials of the EFI system are critical. Attention must be given to the dielectric, triboelectric, and conductivity properties of all elements used in the EFI system where low dielectric, neutral triboelectric, and non-conductive materials are required. A slowly varying electrostatic reference field may be used to reverse and minimize effects of floating gate charging of the FET and leakage currents to facilitate accurate measurements and to provide a very useful “illumination source” for the inspection of objects and volumes.

EFI images reveal the topological nature of electric potentials and a demonstration on locating areas with high electric field magnitudes was provided. EFI images of selected materials provide guidance on materials selection for sensor applications including circuitry, wiring, and structural support systems. EFI imaging of humans was demonstrated and EFI technology was demonstrated showing the feasibility of molecular memory storage. EFI capability extends to subsurface imaging for container inspections and for imaging of hidden objects. Data from an ephemeral e-sensor were presented highlighting its ability to minimize effects due to charging and leakage.

This new EFI capability was demonstrated to reveal characterization of electric charge distribution creating a new field of study embracing areas of interest including ESD mitigation, crime scene forensics, design and materials selection for advanced sensors, dielectric morphology of structures, inspection of containers, inspection for hidden objects, tether integrity, organic molecular memory, and medical diagnostic and treatment efficacy applications such as cardiac polarization wave propagation and electromyography imaging.

REFERENCES

- Blum, D.W., *Electric Field Signature Detection*, U.S. Patent US20120092019, 19 April 2012.
- Dower, R.G., *Apparatus for Electrostatically Imaging the Surface of an Object Located Nearby*, U.S. Patent US5430381, 4 July 1995.
- Generazio, E.R., *Electric Field Quantitative Measurement System and Method*, U.S. Patent 20120199755, 4 February 2011.
- Generazio, E.R., *Ephemeral Electric Potential and Electric Field Sensor*, U.S. Patent US20150137825, 21 May 2015.
- Hassanzadeh, R., D.G. Funderburk, S.A. Schwartz, and E.T. Rock, *Electrostatic Field Gradient Sensor*, U.S. Patent US4931740, 5 June 1990.
- Horowitz, P., and W. Hill, *The Art of Electronics*, second ed., Cambridge University Press, Cambridge, United Kingdom, 1989.
- ITU, *Recommendation B.15: International Telecommunications Union Nomenclature of the Frequency and Wavelength Bands Used in Telecommunications*, International Telecommunications Union, Geneva, Switzerland, 2000.
- Melcher, J.R., *Continuum Electromechanics*, MIT Press, Cambridge, Massachusetts, 1981, p. 1.4.
- NASA, “Quasi-static Electric Field Generator,” *NASA Tech Briefs*, ed. T. Selinsky, Tech Briefs Media Group, New York, New York, 1 November 2014.
- Sothcott, P., *Buried Object Location*, U.K. Patent GB 2132357, 4 July 1984.
- Yang, Y.P., and J. Macnae, *An Apparatus and Method for Detecting an Object in a Medium*, World Intellectual Property Organization Patent WO2002067015, 29 August 2002.
- Zahn, M., “Transform Relationship Between Kerr-effect Optical Phase Shift and Nonuniform Electric Field Distributions,” *IEEE Transactions on Dielectrics and Electrical Insulation*, Vol. 1, No. 2, 1994, pp. 235–246.